



Effect of elliptical dimples on heat transfer performance in a shell and tube heat exchanger

Seyed Ali Abtahi Mehrjardi¹ · Alireza Khademi^{2,3} · Zafar Said^{4,5,6} · Svetlana Ushak⁷ · Ali J. Chamkha⁸

Received: 8 February 2023 / Accepted: 18 April 2023

© The Author(s), under exclusive licence to Springer-Verlag GmbH Germany, part of Springer Nature 2023

Abstract

The numerical simulation of a shell-and-tube heat exchanger (STHE) depends on a large number of computational cells. The number of computational cells increases dramatically with increasing heat transfer surfaces in heat exchangers, such as increasing the number of tubes or using dimples as modified surfaces. Computational cost is one of the critical parameters in many industrial applications for heat exchanger analysis. The present study uses the P-NTU thermal analysis method, proposes correlations to predict heat transfer inside and outside the tubes, and then analyzes the STHE with elliptical dimples. The analytical approach shows 0.8% and 9% errors for two STHEs with specified heat performance, which is entirely acceptable. Also, for the STHE with elliptical dimples, the results indicate a 40.6% increase in the heat capacity of STHE. Increasing the heat capacity of STHE by using modified surfaces such as dimples significantly reduces the dimensions and weight of STHE in industrial applications. Furthermore, the analytical method can be used for different types of dimples with different geometries and arrangements.

Keywords Shell-and-tube heat exchanger (STHE) · P-NTU analysis method · Elliptical dimples · Thermal capacity · Heat transfer performance

Abbreviations

Nomenclature

A	elliptic minor axis (m)
a	constant (dimensionless)
A_c	Cross section area (m ²)
B	elliptic major axis (m)
b	constant (dimensionless)
C	Heat capacity (kJ/K)
C_c	clearance (m)
C_p	specific heat capacity (kJ/kg.K)
D	diameter (m)
d	constant (dimensionless)
G_k	production of turbulent kinetic energy
G_ω	generation of ω
H	depth (m)
h	heat transfer coefficient (W/m ² .K)
K	conductivity (W/m.K)
$LMTD$	Log Mean Temperature Difference
L_{bi}	inlet baffle spacing (m)
L_{bo}	outlet baffle spacing (m)
L_{tp}	tube pitch (m)
N_b	Baffles number
N_p	number of tube passes
N_t	number of tubes

✉ Alireza Khademi
akh95@yorku.ca

¹ Independent Researcher, Tehran, Iran

² Department of Mechanical Engineering, York University, Toronto, ON, Canada

³ Department of Mechanical Engineering, Sharif University of Technology, Tehran, Iran

⁴ Sustainable Energy Development Research Group, College of Engineering, University of Sharjah, Sharjah, United Arab Emirates

⁵ U.S.-Pakistan Center for Advanced Studies in Energy (USPCAS-E), National University of Sciences and Technology (NUST), Islamabad, Pakistan

⁶ Department of Industrial and Mechanical Engineering, Lebanese American University (LAU), Byblos, Lebanon

⁷ Center for Advanced Study of Lithium and Industrial Minerals (CELiMIN) and Departamento de Ingeniería Química y Procesos de Minerales, Universidad de Antofagasta, Campus Coloso, Av. Universidad de Antofagasta, 02800 Antofagasta, Chile

⁸ Faculty of Engineering, Kuwait College of Science and Technology, Doha District 35004, Kuwait

P	dimple longitudinal pitch (m)
q''	heat flux (W/m^2)
R_t	The ratio of tube side to shell side heat capacity
S	distance
T	Temperature (K)
t	Time (s)
U	Overall heat transfer coefficient ($W/m^2 K$)
u	Velocity (m/s)
Y_k	Dissipation of k
Y_ω	Dissipation of ω

Greek symbols

Γ	Production of turbulent kinetic energy
δ_{ij}	Kronecker delta
ε	Turbulent dissipation rate (m^2/s^3)
μ	Velocity (m/s)
ν	Kinematic viscosity (m^2/s)
ρ	Dynamic viscosity ($kg/m.s$)
τ	Stress tensor ($kg/m.s^2$)
ω	Specific rate of dissipation (1/s)
σ_ε	constant
σ_k	constant

Subscripts

e	equivalent
i	inlet
o	outlet
s	shell
t	tube
tu	turbulence

1 Introduction

The use of heat exchangers is prevalent today in a wide variety of industries, including aerospace [1], air-conditioning [2], food [3], chemical plants [4], and automobiles [5]. Shell-and-tube heat exchangers (STHE), which are widely used because they are versatile, easy to maintain, and capable of withstanding high pressure and high temperatures [6], represent about 30 percent of heat exchangers employed [7]. It is, therefore, necessary to concentrate on this device to improve its performance.

The performance of heat exchangers has been improved through numerous experimental studies. El-Said and Al-Sood [8] experimentally investigated an STHE with four baffle layouts to improve its thermal performance. Shirvan et al. [9] proposed a new wavy tube structure in an STHE to study the effects of wavy surface specifications on heat transfer improvement. Rahimi et al. [10] experimentally investigated STHE with spiral tubes filled with phase change material. Although some research on STHEs is performed experimentally, studies are often conducted with CFD, which provides convenience, low costs, and time savings. A numerical study

by Xie et al. [11] evaluated the thermo-fluid character of teardrop-shaped dimples compared to other types. Wang et al. [12] simulated an STHE with staggered baffles to compare the performance of its shell side with two STHEs. Also, an analysis of the parametric relationships between the baffle cut and staggered angle was presented for the STHE with staggered baffles.

In STHEs, baffles are crucial in enhancing the heat transfer coefficient. The baffles cause increasing turbulence intensity and mixing locally by changing fluid movement patterns, which results in a greater heat transfer coefficient. Abbasi et al. [13] employed porous baffles with a special design in STHE, enhancing heat transfer by 11.15%. Arani and Uosofvand [14] examined a new configuration of baffles within an STHE to optimize fluid flow in the shell side accompanied by heat transfer. Meanwhile, the need to improve the thermal performance of heat exchangers has led to the use of nanoparticles [15, 16] and modified surfaces [17, 18].

The use of dimples or fins on the tubes' surface significantly increases their thermal performance [19, 20]. Perwez and Kumar [21] experimentally examined the thermal performance of a spheroidal dimple plate compared to a flat plate in a solar application. There is a significant difference in heat transfer between the spherical dimple plate and the flat plate, as the spherical dimple plate is about 1.51–1.64 times faster than the flat plate. It is estimated that the spherical dimple plate has a thermal efficiency of 23.45% to 35.50% greater than its related flat plate. Manoram et al. [22] studied a heater's thermal efficiency about different dimples parameters. The Nusselt number increased by 2.5 times with the dimpled tube. The dimple is superior as a heat transfer enhancer because it improves thermal efficiency with less friction. Xie et al. [23] numerically investigated the effect of helical dimples in a tube on turbulent heat transfer. The thermal performance of the tube with helical dimples significantly outperformed the plain tube by 120 to 270%.

Several kinds of research with the HTRI, a commercial design program, have been performed to optimize and analyze the performance of STHEs [24, 25]. However, there may be better solutions to use commercial software tools when designing STHEs. In particular applications of STHEs, it is sometimes vital to use the developed surfaces due to weight and volume limitations. The use of dimpled tubes in a compact STHE with many tubes due to the countless heat transfer surfaces makes numerical simulation of this type of exchanger almost impossible. On the other hand, it is necessary to know the thermal performance to design and optimize such STHEs.

This paper aims to provide an alternative method for analyzing the performance of heat exchangers with elliptical dimples. First, relations are provided to predict the Nusselt number (Nu) in terms of Reynolds (Re) and Prandtl (Pr)

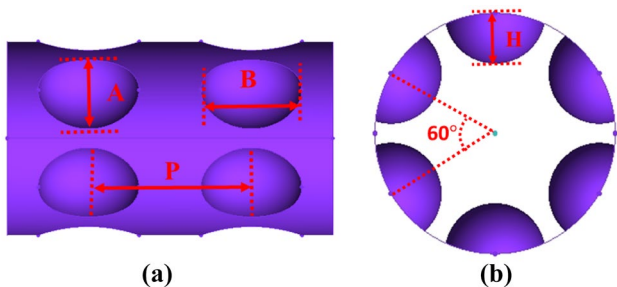


Fig. 1 The schematic **a** cross-sectional and **b** inner side view of the elliptical dimpled tube

numbers for the flow inside the tubes and the shell. Then, the STHE is evaluated using thermal performance analysis methods (P-NTU) [26, 27], an alternative method to heat performance analysis, which is faster and much less expensive than a full-scale numerical simulation of STHEs with the modified surface. The present work simulates the flow inside and across the tube bank with a specific arrangement. Finally, this process is repeated by considering the elliptical dimples on the surface of the tube.

2 Physical model

2.1 Simple tube

The tube used in the simulation has a diameter of 1.6 cm for flow inside the tube and 2 cm for flow across the tube bank when the tubes are in a staggered arrangement. The ratio of tubes transverse distance to the diameter of tubes and the ratio of tubes' longitudinal distance to the diameter are 2.5 and 2.165, respectively, and the tube angle is 30 degrees.

2.2 Dimpled tube

For the dimpled tube, the diameter of the tube and the transverse and longitudinal distances of the tubes are similar to the simple tube. Also, the dimples shown in Fig. 1 are prominent inside the tube, with the geometric characteristics given in Table 1.

Moreover, to examine the effect of longitudinal and transverse distance on heat transfer, which have been selected from Jamil et al. [28] STHE for validation, additional longitudinal and transverse distances are considered according to Table 2.

Table 1 The geometric parameters of the elliptical dimple

Depth (H / D _o)	Radius 1 (A / D _o)	Radius 2 (B / D _o)	Pitch (P / D _o)
0.2105	0.421	0.526	0.842

Table 2 Different tube layouts

$\frac{s_r}{D_o}$	$\frac{s_L}{D_o}$
1.25	1.25
1.33	1.5
1.75	1.75
2	2

2.3 Materials and properties

Water, methanol, and ethanol are selected as working fluids in the STHE because chosen materials cover an extensive range of Pr. Also, the thermophysical properties of water, methanol, and ethanol are listed in Table 3.

Based on the Vogel equation [32], the viscosity of fluids for water, methanol, and ethanol follow Eqs. (1) to (3), respectively.

$$\mu \left(\frac{kg}{m.s} \right) = 0.001 \times \exp \left(-3.7188 + \frac{578.919}{T - 137.546} \right) \quad (1)$$

$$\mu \left(\frac{kg}{m.s} \right) = 0.001 \times \exp \left(-6.7542 + \frac{2337.24}{T + 84.0853} \right) \quad (2)$$

$$\mu \left(\frac{kg}{m.s} \right) = 0.001 \times \exp \left(-7.37 + \frac{2770.25}{T + 74.68} \right) \quad (3)$$

2.4 Data reduction

In the current research, dimensionless numbers are used to reduce the number of data. In addition, numerical solutions can be simplified by using dimensionless parameters, reducing the number of times needed to solve equations. These dimensionless numbers are defined according to Eqs. (4) to (6).

$$Re = \frac{\rho l u}{\mu} \quad (4)$$

$$Pr = \frac{\mu C_p}{K} \quad (5)$$

Table 3 The thermophysical properties of selected fluids

Material	$C_p \left(\frac{kJ}{kg.K} \right)$	$K \left(\frac{W}{m.K} \right)$	$\rho \left(\frac{kg}{m^3} \right)$	References
Methanol	2.84	0.19	750	[29]
Ethanol	3.177	0.18	809.9	[30]
Water	4.182	0.6	998.2	[31]

Table 4 The turbulence models used in numerical simulations

Case	Case	Turbulence model
1	Flow inside the simple tube	Standard k- ω
2	Flow inside the dimpled tube	k- ϵ Realizable
3	Flow across the simple tube bank	k- ϵ Realizable
4	Flow across the dimpled tube bank	Shear Stress Transport (SST) k- ω

$$Nu = \frac{hD}{K} \quad (6)$$

In Eq. (4), l is the inner diameter for flow inside the tube, the outside diameter for flow across the tube bank, and the equivalent diameter for flow on the shell side in the STHE, which is introduced in Eq. (33).

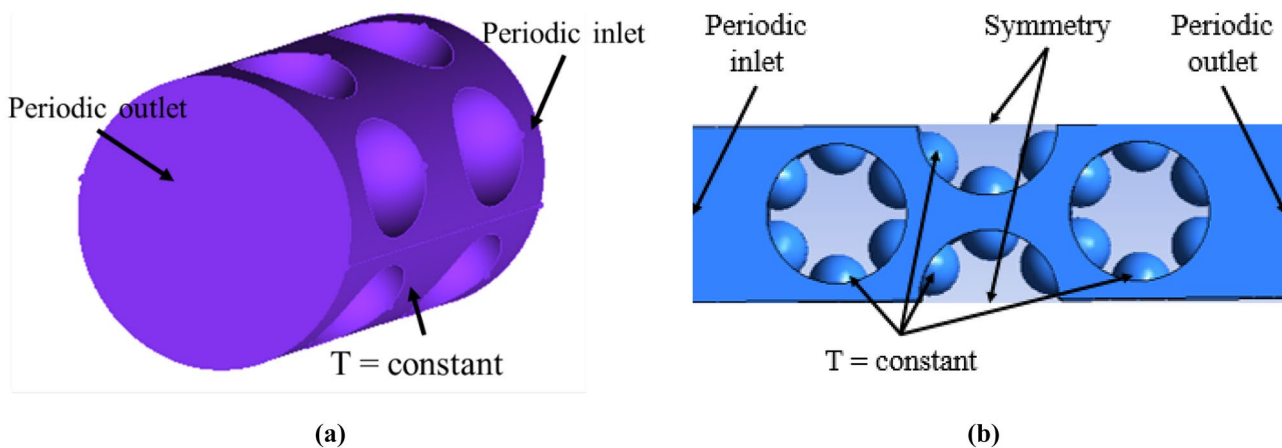
The heat transfer coefficient for the flow inside the tube and the flow across the tube bank is calculated according to Eqs. (7) and (8), respectively.

$$h = \frac{q''}{T_{bulk} - T_{surface}} \quad (7)$$

$$h = \frac{q''}{T_{LMTD}} \quad (8)$$

T_{LMTD} , the log mean temperature difference, in Eq. (8) is defined based on Eq. (9),

$$T_{LMTD} = \frac{T_o - T_i}{\ln\left(\frac{T_{wall} - T_i}{T_{wall} - T_o}\right)} \quad (9)$$

**Fig. 2** Boundary conditions for **a** flow inside the tube and **b** flow across the tube bank

3 Numerical method

3.1 Turbulence model

The selected turbulence models for each mode are listed in Table 4. The basis for their selection for cases 1 to 3 complies with existing experimental and numerical data. The turbulence model for case 4 is selected based on the model's accuracy in predicting heat transfer for the dimple case.

For cases 2 and 3, functions used near the wall are enhanced wall treatment.

3.2 Boundary conditions

For flow inside a simple and dimpled tube, the boundary condition for the inlet and outlet of the tube is periodic, and a constant temperature boundary condition is set for the tube wall. The boundary conditions assumed for flow across the tube bank are shown in Fig. 2.

The boundary conditions are the same for a simple tube (without dimples). In the numerical simulations, the wall temperature varied between 290 and 350 K. The fluid inlet temperature ranged from 280 to 340 K. Existence of periodic boundary conditions in the inlet and outlet of geometries causes complete thermal development for the flow inside the tube, and considering a large number of tubes for flow across tube bank and eliminates the effects related to the number of tubes in heat transfer.

Table 5 The grid independence validation of flow inside the dimpled tube

Grid	Number of computational cells	Nu	Different %
(1)	201,627	208	13.4
(2)	302,823	226.3	5.8
(3)	404,707	238.1	0.9
(4)	801,425	240.2	0

4 Governing equations and assumption

As mentioned earlier, k-ε realizable is chosen to predict heat transfer inside the dimpled tube and flow across the simple tube bank. The associated governing equations are as follows.

The continuity equation [11]:

$$\frac{\partial}{\partial x_i} (\rho u_i) = 0 \tag{10}$$

The momentum equation [11]:

$$\frac{\partial}{\partial x_j} (\rho u_i u_j) = -\frac{\partial p}{\partial x_i} + \frac{\partial}{\partial x_j} (\mu + \mu_{tu}) \left(\frac{\partial u_i}{\partial x_j} + \frac{\partial u_j}{\partial x_i} \right) \tag{11}$$

The energy equation [11]:

$$\frac{\partial}{\partial x_i} (u_i T) = \frac{\partial}{\partial x_i} \left[\left(\frac{\mu}{Pr} + \frac{\mu_{tu}}{Pr_{tu}} \right) \frac{\partial T}{\partial x_i} \right] \tag{12}$$

And transport equations for the k-ε realizable turbulence model described in Eqs. (13) to (16) [11],

$$\frac{\partial}{\partial x_j} (\rho k u_j) = \frac{\partial}{\partial x_j} \left[\left(\mu + \frac{\mu_{tu}}{\sigma_k} \right) \frac{\partial k}{\partial x_j} \right] + \Gamma - \rho \epsilon \tag{13}$$

$$\frac{\partial}{\partial x_j} (\rho \epsilon u_j) = \frac{\partial}{\partial x_j} \left[\left(\mu + \frac{\mu_{tu}}{\sigma_\epsilon} \right) \frac{\partial \epsilon}{\partial x_j} \right] + C_1 \Gamma \epsilon - C_2 \frac{\epsilon^2}{k + \sqrt{v \epsilon}} \tag{14}$$

$$\Gamma = -\frac{\overline{u_i u_j} \frac{\partial u_i}{\partial x_j}}{\rho} = \frac{\mu_{tu}}{\rho} \left(\frac{\partial u_i}{\partial x_j} + \frac{\partial u_j}{\partial x_i} \right) \frac{\partial u_i}{\partial x_j} \tag{15}$$

Table 6 The grid independence validation of flow across the dimpled tube bank

Grid	Number of computational cells	Nu	Different %
(1)	425,211	35.7	11.5
(2)	817,416	38.1	5.7
(3)	1,203,352	40.1	0.7
(4)	1,617,127	40.4	0

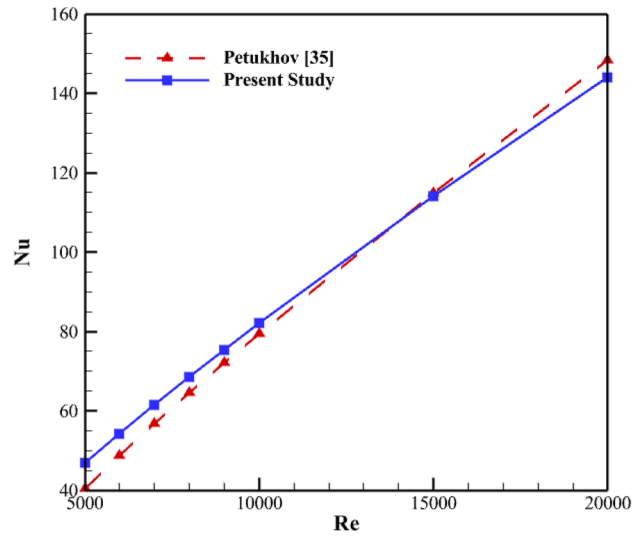


Fig. 3 Comparison of Nusselt number in the present study with Petukhov [37]

$$C_1 = \max \left[0.43 \frac{\mu_t}{\mu_t + 5} \right], C_2 = 1.0, \sigma_k = 1.0, \sigma_\epsilon = 1.2, \mu_{tu} = \rho C_\mu \frac{k^2}{\epsilon} \tag{16}$$

For predicting heat transfer for flow inside the simple tube, k-ω Standard is chosen for turbulence modeling. The related transport Equation for this turbulence model is as follows in Eqs. (17) to (20) [33]:

$$\frac{D\rho k}{Dt} = \tau_{ij} \frac{\partial u_i}{\partial x_j} - \beta^* \rho \omega k + \frac{\partial}{\partial x_j} \left[(\mu + \sigma_{k1} \mu_{tu}) + \frac{\partial k}{\partial x_j} \right] \tag{17}$$

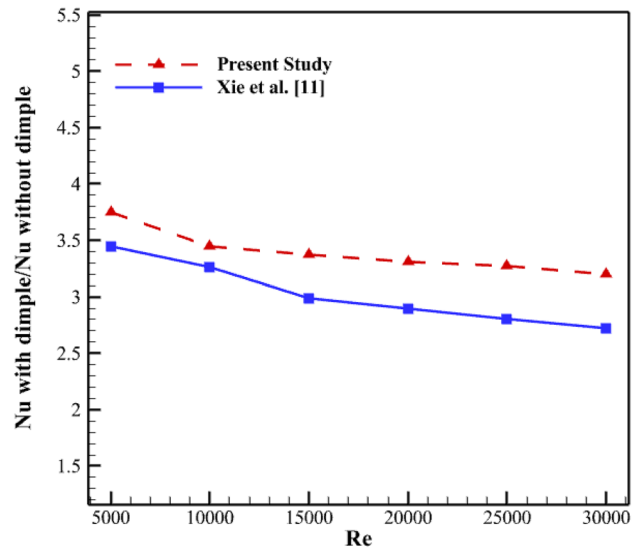


Fig. 4. Comparison of Nusselt number in the present study with Xie et al. [11]

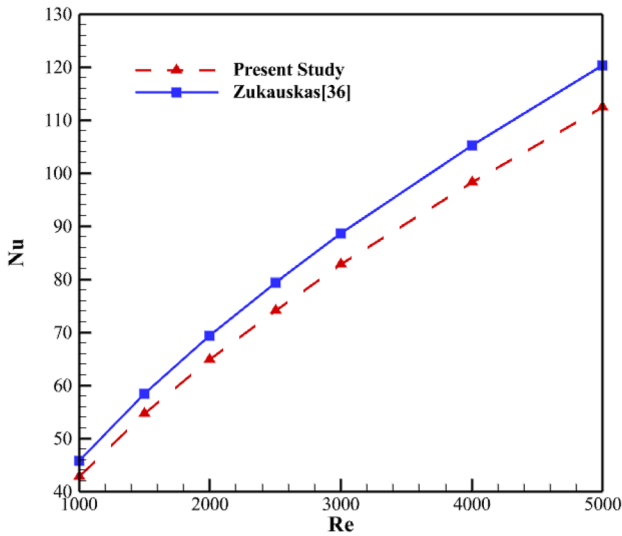


Fig. 5. Comparison of Nusselt number in the present study with Zukauskas [36]

$$\frac{D\rho\omega}{Dt} = \frac{\gamma_1}{v_t} \tau_{ij} \frac{\partial u_i}{\partial x_j} - \beta_1 \rho \omega^2 + \frac{\partial}{\partial x_j} \left[(\mu + \sigma_{\omega 1} \mu_{tu}) + \frac{\partial \omega}{\partial x_j} \right] \quad (18)$$

$$v_t := \frac{\mu_{tu}}{\rho} = \frac{k}{\omega} \quad (19)$$

$$\tau_{ij} = \mu_{tu} \left(\frac{\partial u_i}{\partial x_j} + \frac{\partial u_j}{\partial x_i} - \frac{2}{3} \frac{\partial u_k}{\partial x_k} \delta_{ij} \right) - \frac{2}{3} \rho k \delta_{ij} \quad (20)$$

And, for heat transfer simulation for flow across tube bank, k- ω Shear Stress Transport (SST) is chosen for turbulence modeling; the transport Equations for this turbulence model follow in Eqs. (21) to (27) [34]:

$$\frac{\partial}{\partial x_i} (\rho k u_i) = \frac{\partial}{\partial x_j} \left(\left(\mu + \frac{\mu_{tu}}{\sigma_k} \right) \frac{\partial k}{\partial x_j} \right) + \widetilde{G}_k - Y_k + S_k \quad (21)$$

$$\frac{\partial}{\partial x_i} (\rho \omega k u_i) = \frac{\partial}{\partial x_j} \left(\left(\mu + \frac{\mu_{tu}}{\sigma_\omega} \right) \frac{\partial \omega}{\partial x_j} \right) + G_\omega - Y_\omega + D_\omega + S_\omega \quad (22)$$

$$\widetilde{G}_k = \min(G_k, 10\beta^* k \omega) \quad (23)$$

$$G_k = -\rho \overline{u_i' u_j'} \left(\frac{\partial u_j}{\partial x_i} \right) \quad (24)$$

$$Y_k = \rho \beta^* k \omega \quad (25)$$

$$Y_\omega = \rho \beta \omega^2 \quad (26)$$

$$\mu_{tu} = \alpha^* \frac{\rho k}{\omega} \quad (27)$$

Thermal effectiveness is defined as P, the temperature effectiveness. An exchanger with two fluids has a different exchange rate for each fluid. Regardless of whether it is a hot or cold fluid, P is the ratio of the rise or drop of the fluid temperature to the difference between their inlet temperatures:

$$P_t = \frac{T_{t,o} - T_{t,i}}{T_{s,i} - T_{t,i}} \quad (28)$$

where R_t , the heat capacity rate ratios, are:

$$R_t = \frac{C_t}{C_s} = \frac{T_{s,i} - T_{s,o}}{T_{t,o} - T_{t,i}} \quad (29)$$

NTU is also provided for each fluid by the following,

$$NTU_t = \frac{UA}{C_t} \quad (30)$$

In this method, to analyze a heat exchanger, it is divided into a number of blocks. The parameter P for each block is calculated based on the orientation of fluids 1 (tube side) and 2 (shell side) (counter/parallel/crossflow). In the following, the method of calculating P based on the arrangement of fluids 1 (unmixed) and 2 (mixed) relatives to each other is presented for crossflow.

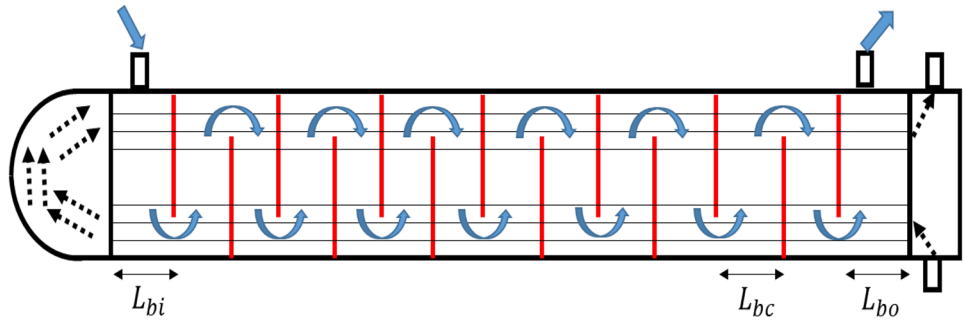
$$P_1 = \frac{1 - \exp(-KR_t)}{R_t} \quad (31)$$

$$K = 1 - \exp(NTU_t) \quad (32)$$

Table 7 The specification of Jamil et al. [28] STHE

Parameter	Value
Mass flow rate (shell/tube), kg/s	27.8/68.9
Shell side temperature (inlet, T_{si} /outlet, T_{so}), K	368.15/313.15
Tube side temperature (inlet, T_{ti} /outlet, T_{to}), K	298.15/313.15
Fluid (shell/tube)	Methanol/Water
Tube layout, degree	30°
Number of tube passes, N_p	2
Tube inner diameter, D_{ii} , m	0.016
Tube outer diameter, D_{to} , m	0.02
Baffles number, N_b	13
Baffle spacing, $L_{bi}=L_{bc}=L_{bo}$, m	0.356
Tube pitch, L_{ip} , m	0.025
Shell diameter, D_s , m	0.894
Number of tubes, N_t	918

Fig. 6 The schematic of Jamil et al. [28] STHE for validation in the current study



The hydraulic diameter of the shell in a staggered arrangement is equal to:

$$D_e = \frac{4 \left(\frac{\sqrt{3}P_t^2}{4} - \frac{\pi d_o^2}{8} \right)}{\pi d_{outer}} \quad (33)$$

Also, the cross-sectional area of fluid flow in a shell is obtained from the following equation:

$$A_c = \frac{D_s C_c B}{P_t} \quad (34)$$

$$Re_s = \frac{\rho u D_e}{\mu} = \frac{\dot{m} D_e}{A_c \mu} \quad (35)$$

Clearance, the distance between outer surface of two adjacent tubes, is calculated in this way:

$$C_c = P_t - d_o \quad (36)$$

Finally, the overall heat transfer coefficient is as follows,

$$\frac{1}{U_{inner}} = \frac{d_{inner}}{h_{outer} d_{outer}} + \frac{d_{inner} \ln \left(\frac{d_{outer}}{d_{inner}} \right)}{2k_{wall}} + \frac{1}{h_{inner}} \quad (37)$$

5 Heat transfer prediction

The general form of Nusselt number behavior based on Re and Pr, dimensionless numbers, follows Eq. (38) trend for flow inside the tube. The reason for choosing this trend is that regression is close to 1, which shows that the simulation data strongly follows this trend and can be used confidently to predict heat transfer for data other than the simulation data.

$$Nu = a \times Re^b \times Pr^c \quad (38)$$

Coefficients a, b, and c are unknown constants in Eq. (38) according to the general form of Dittus-Boelter [35]

correlation and are obtained by minimizing the squared error for each case.

In the case of flow across tube banks, the heat transfer can be expressed through Eq. (39) according to the general form of the Zukauskas [36] correlation. This equation is particularly suitable for predicting heat transfer as it exhibits a regression close to 1, in line with the Nu number trend for flow across tube banks. The coefficients a, b, c, e, and f in Eq. (39) must be determined by minimizing the squared error for each case to predict the heat transfer accurately.

$$Nu = a \times Re^b \times Pr^c \left(\frac{S_L}{D_o} \right)^e \times \left(\frac{S_T}{D_o} \right)^f \quad (39)$$

Dimensionless heat transfer for the flow inside the simple tube and flow across the simple tube bank is according to Eqs. (40) and (41).

$$Nu = 0.02379 \times Re^{0.8105} \times Pr^{0.3756} \quad (40)$$

$$Nu = 0.2617 \times Re^{0.5963} \times Pr^{0.3568} \times \left(\frac{S_L}{D_o} \right)^{0.4} \times \left(\frac{S_T}{D_o} \right)^{-0.1} \quad (41)$$

And, dimensionless heat transfer for the flow inside the dimpled tube and flow across the dimpled tube bank is according to Eqs. (42) and (43).

$$Nu = 0.162 \times Re^{0.745} \times Pr^{0.3117} \quad (42)$$

$$Nu = 0.527 \times Re^{0.8337} \times Pr^{0.313} \times \left(\frac{S_L}{D_o} \right)^{0.35} \times \left(\frac{S_T}{D_o} \right)^{-0.12} \quad (43)$$

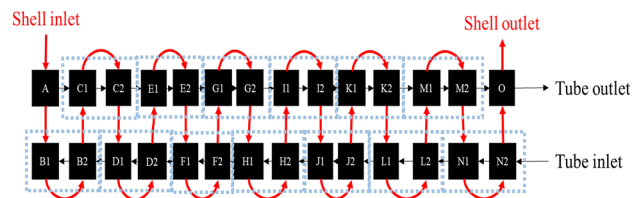
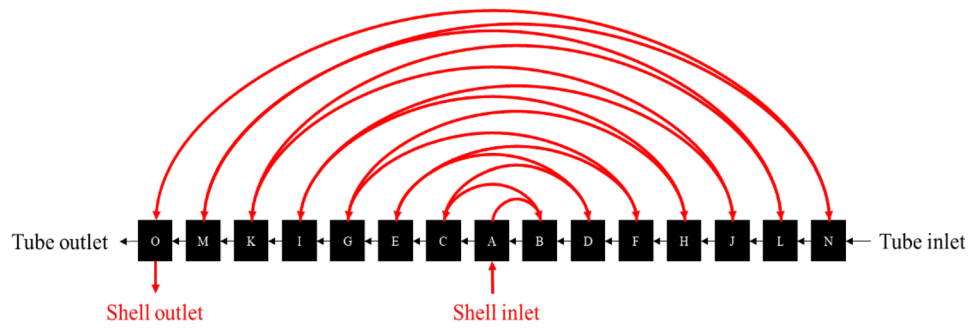


Fig. 7 The schematic of Jamil et al. [28] STHE divided into several blocks

Fig. 8 The arrangement of adjacent blocks for Jamil et al. [28] STHE



Forty data from numerical simulation have been used to propose Eqs. (40) to (43) for Nu number in terms of Re and Pr for different cases.

6 Validation

6.1 Grid independence verification

To ensure grid independency, four types of grids with different numbers of computational cells are considered for each simulation mode case, shown in Table 5, and the differences are compared with the denser ones. In order to investigate grid independence for flow inside the tube, a specific set of boundary conditions was established. For this study, Re was set to 8000, and Pr was set to 6.98. On the other hand, for flow across the tube bank, Re and Pr were considered as 1000 and 6.98, respectively. These values were chosen for the purpose of examining the level of grid independence in the simulated flow. In the study of grid independence for flow inside tubes and across tube banks, the results are presented in Table 5 and Table 6, respectively.

According to the results of Tables 5 and 6, the number of computational cells for the grid (3) can be trusted for the flow inside the tube and the flow across the tube bank.

6.2 Model validation

In this section, the results of numerical solutions to predict heat transfer of flow for different modes consisting of flow inside a simple tube, the flow inside a dimpled tube, and crossflow over a tube bank are validated by the results of previous studies. The operating fluid and Pr are chosen water and 6.98, respectively.

Table 8 Comparison of the results of the present study and Jamil et al. [28] STHE

	T_{so} (K)	T_{to} (K)	Heat capacity (kW)	Different (%)
Present study	318.3	311.8	3933.1	9%
Jamil et al. [28]	313.15	313.15	4322.1	--

First, to study the flow inside a simple tube shown in Fig. 3, the Re range is chosen from 5000 to 20000, which compares the results of the numerical simulations in the present study with the results of the Petukhov [37] research. The comparison between the results obtained from the present numerical simulation and Petukhov's [37] findings, as shown in Fig. 3, reveals a maximum difference of 12%, which is considered acceptable. Additionally, Fig. 3 illustrates that the calculated Nu number tends to underestimate lower Re numbers and overestimate higher Re numbers. This trend highlights the sensitivity of the Nu number with respect to the Re number because of the implemented turbulence model.

The study compared the Nu number ratio of a dimpled tube to a simple tube, as depicted in Fig. 4, within the range of Re from 5000 to 30000. The results were compared with the research conducted by Xie et al. [11], and slight differences were noted (maximum of about 14%). Nonetheless, this level of variation is considered acceptable. Moreover, these findings suggest that the k-ε Realizable turbulence model employed in this configuration has been demonstrated earlier is appropriate since the acceptable error in the entire range of simulation.

Table 9 The specification of Leoni et al. [25] STHE

Parameter	Value
Mass flow rate (shell/tube), kg/s	3.5/1.59
Shell side temperature (inlet, T_{si} /outlet, T_{so}), K	363.15/380.18
Tube side temperature (inlet, T_{ti} /outlet, T_{to}), K	463.15/443.15
Fluid (shell/tube)	Crude oil/Water
Tube layout, degree	30°
Number of tube passes, N_p	1
Tube inner diameter, D_{ii} , m	0.01575
Tube outer diameter, D_{to} , m	0.019
Baffles number, N_b	4
Baffle spacing, L_{bc} , m	0.160
Inlet and outlet spacing $L_{bi} = L_{bo}$, m	0.290
Tube pitch, L_{ip} , m	0.025
Shell diameter, D_s , m	0.205
Number of tubes, N_t	43

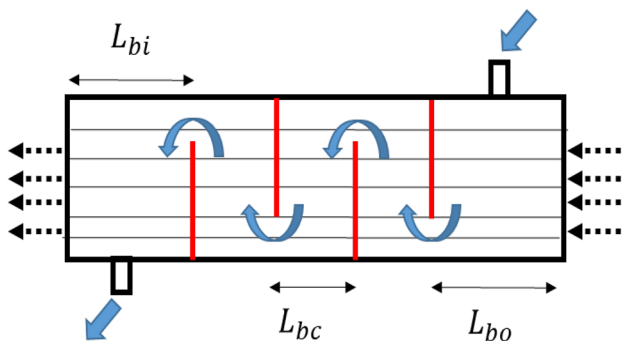


Fig. 9 The schematic of Leoni et al. [25] STHE for validation in the current study

Figure 5 compares the results obtained in this study with those reported in a previous work by Zukauskas [36], considering a Reynolds number (Re) range of 1000 to 5000. The maximum observed error is 6.6%, with a significantly lower average error. These findings indicate a good agreement between the results of our study and those obtained by Zukauskas [36], as further supported by Table 4. The results also suggest that the k- ω SST model is appropriate for simulating flow across a tube bank. Notably, the difference in percentage error between our study and that of Zukauskas [36] did not vary significantly with increases in the Re number range considered in the simulation, and it hasn't resulted in more or less error in the range of simulation.

Therefore, the results obtained in the present study can be used in the simulated range because comparing the results of the present study with the results of the reference research [11, 36, 37] to examine accuracy shows a good fit.

7 Analytical approach

In this section, first, the reliability of the P-NTU algorithm is evaluated by the analytical solution of Jamil et al. [28] STHE, which is the validation reference of many studies,

Table 10 Comparison of the results of the present study and Leoni et al. [25] STHE

Cases	T_{so} (K)	T_{to} (K)	Heat capacity (kW)
Leoni et al. [25]	380.18	443.15	125.46
Present study without dimple	379.31	444.44	124.41
Present study with dimple	387.43	435.03	176.4

including [38–40]. Then the effect of using the elliptical dimple on the Xie et al. [11] in increasing the thermal capacity of the STHE is evaluated. The specifications of Jamil et al. [28] STHE is given in Table 7, and its schematic is in Fig. 6.

To derive an analytical solution for the STHE, it is necessary to treat the point of contact between the tubes and the shell fluid in each section as a discrete block. The arrangement of these blocks is determined based on the point of contact between the shell side flow and the tubes. Figure 7, adapted from Jamil et al. [28], illustrates how the STHE is divided into multiple blocks.

Depending on the arrangement of the adjacent block, the equivalent temperature effectiveness coefficient should be calculated for the whole STHE, where more details are shown in Fig. 8.

Based on the Equation required for heat exchanger analysis by the P-NTU method and equivalent temperature effectiveness coefficient to the results of heat exchanger performance analysis and the existing results of Jamil et al. [28] research is given in Table 8.

According to Table 8, the methods used in the present study and Jamil et al. [28] results are 9% different. Therefore, the results of this study's method (P-NTU) can be trusted. The origin of this error can be attributed to using the P-NTU method in the current study, which utilizes an empirical correlation that differs from the one used in the Bell-Delaware method employed by Jamil et al. [28] in their STHE solution. Additionally, the assumption made by the

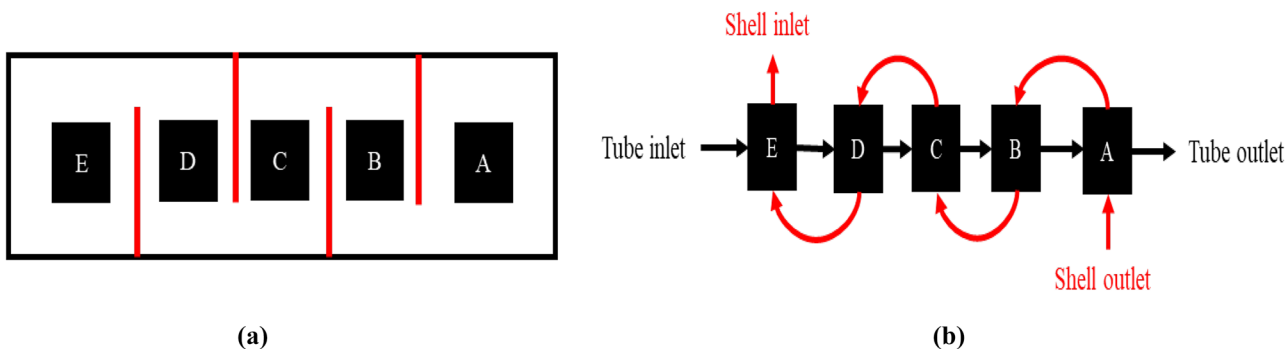


Fig. 10 The schematic of Leoni et al. [25] STHE, (a) divided into several blocks (b) arrangement of the adjacent block

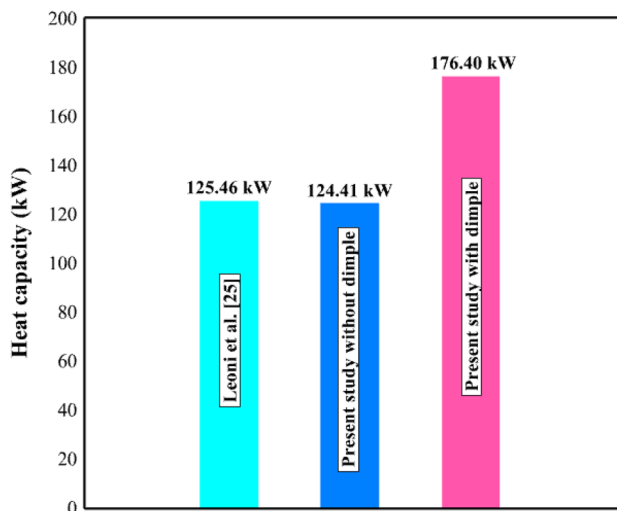


Fig. 11 Comparison between Leoni et al. [25] STHE and present study and evaluation dimple effect

P-NTU method that the flow direction over the tube is completely perpendicular may not hold in reality, contributing to the error in the solution.

In the following, the STHE of Leoni et al. [25] is investigated in terms of thermal performance by the P-NTU method with and without the elliptical dimpled tube. The specifications Leoni et al. [25] STHE is given in Table 9, and its schematic is in Fig. 9.

Figure 10 shows how the Leoni et al. [25] STHE is divided into several blocks and the arrangement of the blocks together.

In their research, Leoni et al. [25] analyzed the thermal performance of the STHE using ANSYS and HTRI software. The results of Leoni et al. [25], in their research considering simple tubes and the consequences of Leoni STHE heat capacity in the present study assessing simple tube and dimpled tube introduced in Table 1, are presented in Table 10. According to Fig. 11, dimples on the tube surface have increased the STHE heat capacity by 40.6% without increasing its dimensions and weight.

8 Conclusions

The present study analytically evaluates the effect of elliptical dimples on increasing the heat capacity of STHE by the P-NTU method and proposes the correlations for predicting heat transfer according to Re and Pr. At first, the turbulence models, including $k-\varepsilon$ realizable, $k-\omega$ standard, and $k-\omega$ SST, are used to validate the heat transfer inside and outside the tube, which is compared with the results of previous references to ensure the accuracy of the proposed correlations. Then, the thermal performance of the STHE

is verified using the provided correlations and the P-NTU solution method. Accordingly, the effect of the specified dimple on thermal performance is examined. The primary findings of the current study are as follows:

1. Implementing the analytical method has led to a marked decrease in computational expenses by avoiding using a vast number of computational cells. A study conducted by Leoni et al. [25] revealed that while the STHE with processor Intel Core i7 3.4 GHz and 8 GB RAM took approximately 3-5 days, the P-NTU method solved in just a few seconds. Notably, when dealing with modified surfaces, the computational domain requires even more computational cells, increasing the time needed for convergence. As a result, the CFD approach may only be feasible for some industrial applications.
2. The analytical method has an error of up to 9% for STHEs studied in the present study, which is acceptable.
3. The elliptical dimple configuration described in the present study increases STHE heat capacity by 40.6%.
4. Mitigating the size and weight of STHE by using dimples is essential in industrial applications.
5. The method used here is reliable for investigating the effect of other dimple configurations.

Funding This work has been funded by ANID/FONDAP 15110019 SERC-Chile project.

References

1. Mekki BS, Langer J, Lynch S (2021) Genetic algorithm based topology optimization of heat exchanger fins used in aerospace applications. *Int J Heat Mass Transf* 170
2. D'Agostino D, Greco A, Masselli C, Minichiello F (2020) The employment of an earth-to-air heat exchanger as pre-treating unit of an air conditioning system for energy saving: A comparison among different worldwide climatic zones. *Energy Build* 229
3. Dekhil MA, Tala JVS, Bulliard-Sauret O, Bougeard D (2020) Development of an innovative heat exchanger for sensible heat storage in agro-food industry. *Appl Therm Eng* 177
4. Ni T-W, Fei J-L, Wang S-H, Gong Y, Yang Z-G (2020) Failure analysis on unexpected perforation of heat exchanger tube in methacrylic acid reboiler of specialty chemical plant. *Eng Fail Anal* 108
5. Habibian S, Abolmaali AM, Afshin H (2018) Numerical investigation of the effects of fin shape, antifreeze and nanoparticles on the performance of compact finned-tube heat exchangers for automobile radiator. *Appl Therm Eng* 133:248–260
6. Wang J, Liu T, Xu C, Wang J, Feng L-F (2021) Numerical investigation on hydrodynamics and heat transfer of highly viscous fluid in Sulzer mixer reactor. *Int J Heat Mass Transf* 171
7. He L, Li P (2018) Numerical investigation on double tube-pass shell-and-tube heat exchangers with different baffle configurations. *Appl Therm Eng* 143:561–569
8. El-Said EM, Abou Al-Sood M (2019) Shell and tube heat exchanger with new segmental baffles configurations: a

- comparative experimental investigation. *Appl Therm Eng* 150:803–810
9. Shirvan KM, Mamourian M, Esfahani JA (2018) Experimental investigation on thermal performance and economic analysis of cosine wave tube structure in a shell and tube heat exchanger. *Energy Convers Manage* 175:86–98
 10. Rahimi M, Hosseini M, Gorzin M (2019) Effect of helical diameter on the performance of shell and helical tube heat exchanger: an experimental approach. *Sustain Cities Soc* 44:691–701
 11. Xie S, Liang Z, Zhang J, Zhang L, Wang Y, Ding H (2019) Numerical investigation on flow and heat transfer in dimpled tube with teardrop dimples. *Int J Heat Mass Transf* 131:713–723
 12. Wang X, Zheng N, Liu Z, Liu W (2018) Numerical analysis and optimization study on shell-side performances of a shell and tube heat exchanger with staggered baffles. *Int J Heat Mass Transf* 124:247–259
 13. Abbasi HR, Sedeh ES, Pourrahmani H, Mohammadi MH (2020) Shape optimization of segmental porous baffles for enhanced thermo-hydraulic performance of shell-and-tube heat exchanger. *Appl Therm Eng* 180
 14. Arani AAA, Uosofvand H (2021) Double-pass shell-and-tube heat exchanger performance enhancement with new combined baffle and elliptical tube bundle arrangement. *Int J Therm Sci* 167
 15. Esfahani J, Akbarzadeh M, Rashidi S, Rosen M, Ellahi R (2017) Influences of wavy wall and nanoparticles on entropy generation over heat exchanger plat. *Int J Heat Mass Transf* 109:1162–1171
 16. Seyednezhad M, Sheikholeslami M, Ali JA, Shafee A, Nguyen TK (2020) Nanoparticles for water desalination in solar heat exchanger. *J Therm Anal Calorim* 139(3):1619–1636
 17. Zheng N, Liu W, Liu Z, Liu P, Shan F (2015) A numerical study on heat transfer enhancement and the flow structure in a heat exchanger tube with discrete double inclined ribs. *Appl Therm Eng* 90:232–241
 18. Mangrulkar CK, Dhoble AS, Chakrabarty SG, Wankhede US (2017) Experimental and CFD prediction of heat transfer and friction factor characteristics in cross flow tube bank with integral splitter plate. *Int J Heat Mass Transf* 104:964–978
 19. Xu J, Li J, Ding Y, Fu Q, Cheng M, Liao Q (2018) Numerical simulation of the flow and heat-transfer characteristics of an aligned external three-dimensional rectangular-finned tube bank. *Appl Therm Eng* 145:110–122
 20. Kurşun B (2019) Thermal performance assessment of internal longitudinal fins with sinusoidal lateral surfaces in parabolic trough receiver tubes. *Renewable Energy* 140:816–827
 21. Perwez A, Kumar R (2019) Thermal performance investigation of the flat and spherical dimple absorber plate solar air heaters. *Sol Energy* 193:309–323
 22. Manoram R, Moorthy RS, Ragnathan R (2021) Investigation on influence of dimpled surfaces on heat transfer enhancement and friction factor in solar water heater. *J Therm Anal Calorim* 145(2):541–558
 23. Xie S, Guo Z, Gong Y, Dong C, Liu J, Ren L (2022) Numerical investigation of thermal-hydraulic performance of a heat exchanger tube with helical dimples. *Int J Therm Sci* 177
 24. Caputo AC, Pelagagge PM, Salini P (2015) Heat exchanger optimized design compared with installed industrial solutions. *Appl Therm Eng* 87:371–380
 25. Leoni GB, Klein TS, de Andrade Medronho R (2017) Assessment with computational fluid dynamics of the effects of baffle clearances on the shell side flow in a shell and tube heat exchanger. *Appl Therm Eng* 112:497–506
 26. Kandlikar SG, Shah RK (1989) Asymptotic effectiveness-NTU formulas for multipass plate heat exchangers 111(2):314–321. <https://doi.org/10.1115/1.3250679>
 27. Pignotti A, Shah R (1992) Effectiveness-number of transfer units relationships for heat exchanger complex flow arrangements. *Int J Heat Mass Transf* 35(5):1275–1291
 28. Jamil MA, Goraya TS, Shahzad MW, Zubair SM (2020) Exergo-economic optimization of a shell-and-tube heat exchanger. *Energy Convers Manage* 226
 29. Sadeghzadeh H, Ehyaei M, Rosen M (2015) Techno-economic optimization of a shell and tube heat exchanger by genetic and particle swarm algorithms. *Energy Convers Manage* 93:84–91
 30. Liu H, Cai C, Yin H, Luo J, Jia M, Gao J (2018) Experimental investigation on heat transfer of spray cooling with the mixture of ethanol and water. *Int J Therm Sci* 133:62–68
 31. Mehrjardi SAA, Khademi A, Ushak S, Alotaibi S (2022) Melting process of various phase change materials in presence of auxiliary fluid with sinusoidal wall temperature. *J Energy Stor* 52:104779. <https://doi.org/10.1016/j.est.2022.104779>
 32. Nascimento MLF, Aparicio C (2007) Data classification with the Vogel–Fulcher–Tammann–Hesse viscosity equation using correspondence analysis. *Physica B* 398(1):71–77
 33. Menter F (1993) Zonal two equation kw turbulence models for aerodynamic flows. In 23rd Fluid Dyn Plasmadynamics Lasers Conf p. 2906
 34. Moghaddaszadeh N, Rashidi S, Esfahani JA (2018) Potential of gear-ring turbulator in three-dimensional heat exchanger tube from second law of thermodynamic viewpoint. *Internat J Numer Methods Heat Fluid Flow* 29(4):1526–1543
 35. Dittus F, Boelter L (1930) Publications on engineering. University of California, Berkeley 2(13):443–461
 36. Žukauskas A (1972) Heat transfer from tubes in crossflow. In *Adv Heat Transf* 8(Elsevier):93–160
 37. Petukhov BS (1970) Heat transfer and friction in turbulent pipe flow with variable physical properties. *Adv Heat Transf* 6:503–564
 38. Sinnott R, Towler G (2019) *Chemical engineering design: SI Edition*. Butterworth-Heinemann
 39. Tariq R et al (2021) Artificial intelligence assisted techno-economic optimization scenarios of hybrid energy systems for water management of an isolated community. *Sustainable Energy Technol Assess* 48
 40. Gu X, Wang G, Zhang Q, Chen C, Li N, Chen W (2022) Fluid-structure interaction analysis of heat exchanger with torsional flow in the shell side. *J Mech Sci Technol* 36(1):479–489

Publisher's Note Springer Nature remains neutral with regard to jurisdictional claims in published maps and institutional affiliations.

Springer Nature or its licensor (e.g. a society or other partner) holds exclusive rights to this article under a publishing agreement with the author(s) or other rightsholder(s); author self-archiving of the accepted manuscript version of this article is solely governed by the terms of such publishing agreement and applicable law.